THE JOURNAL OF PHYSICAL CHEMISTRY C

Article

pubs.acs.org/JPCC

Effects of Surface Blocking Layer of Sb_2S_3 on Nanocrystalline TiO_2 for $CH_3NH_3PbI_3$ Perovskite Solar Cells

Seigo Ito,*[,†] Soichiro Tanaka,[†] Kyohei Manabe,[‡] and Hitoshi Nishino[‡]

[†]Department of Electric Engineering and Computer Science, Graduate School of Engineering, University of Hyogo, 2167 Shosha, Himeji, Hyogo 671-2280, Japan

[‡]Energy Technology Laboratories, Osaka Gas Co., Ltd., 6-19-9 Torishima, Konohana-Ku, Osaka 554-0051, Japan

ABSTRACT: Sb_2S_3 layers were inserted at the interface between TiO_2 and $CH_3NH_3PbI_3$ perovskite to create $CH_3NH_3PbI_3$ solar cells using inorganic hole transporting material (CuSCN). The $CH_3NH_3PbI_3$ layer was spin-coated by a one-drop method onto the nanocrystalline TiO_2 layer. The photoenergy conversion efficiencies were improved with Sb_2S_3 layers (the best efficiency: 5.24%). During the light exposure test without encapsulation, the $CH_3NH_3PbI_3$ solar cells without Sb_2S_3 deteriorated to zero efficiency in 12 h and were completely changed from black to yellow because the perovskite $CH_3NH_3PbI_3$ was changed to hexagonal PbI_2. With Sb_2S_3, on the other hand, the $CH_3NH_3PbI_3$ solar cells became stable against light exposure without encapsulation, which did not change the crystal structure or the wavelength edges of absorption and IPCE. Therefore, it was believed that degradation can occur at the interface between TiO_2 and $CH_3NH_3PbI_3$.

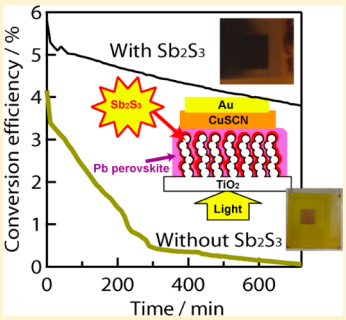

INTRODUCTION

Recently, solid-state printed solar cells using $CH_3NH_3PbX_3$ (X: halide) perovskite as a photoabsorber have been intensively investigated, by performing high photoenergy-conversion efficiencies of 9.7−15.7% using low-cost processes (spin coating).[1−6] However, their stability has been ambiguous. At first, the stability of $CH_3NH_3PbX_3$ solar cells have been reported without encapsulation stored in the dark.[1,3] Under constant illumination at 100 mW cm^{-2}, the $CH_3NH_3PbX_3$ stability test was performed with encapsulation.[2,4] Although the $CH_3NH_3PbX_3$ exhibited very promising long-term stability, sealing by organic materials cannot be seamless against water and oxygen. Therefore, it is important to evaluate the stability under light irradiation without encapsulation. In this work, we investigated the stability of the perovskite $CH_3NH_3PbI_3$ under one sun irradiation (AM 1.5) without encapsulation.

In order to improve the stability of solar cells against light irradiation, the passivation of the TiO_2 photocatalytic effect should be considered using the surface blocking layer. Moreover, in the reports of dye-sensitized solar cells (DSCs) and extremely thin absorber (ETA) solar cells, which have been composed of nanocrystalline TiO_2 photoelectrodes like $CH_3NH_3PbX_3$ perovskite solar cells, the surface blocking layer can improve the photovoltaic characteristics by blocking the charge recombination between electrons in TiO_2 and holes in hole-transporting materials (HTM).[7−9] Hence, the surface blocking layer on TiO_2 has two blocking functions: the blockings of the TiO_2 photocatalytic effect and the charge recombination in TiO_2 and HTM.

Usually, metal oxides are utilized for DSCs and ETA cells for such a surface blocking layer. In this report, however, Sb_2S_3 has been utilized as the surface blocking layer due to the facile fabrication on the nanocrystalline TiO_2 layer, the photostability, and the energy diagram to transport electrons from $CH_3NH_3PbI_3$ to TiO_2 (Figure 1), which can extend the distance between electrons and holes. Although there is a small energy wall between the conduction bands (spike) from $CH_3NH_3PbI_3$ to Sb_2S_3 (0.2 eV), this spike is quite similar to the energy diagrams in $Cu(In,Ga)(S,Se)_2$ (CIGS) solar cells between CIGS and buffering sulfides and can enhance the photoenergy conversion efficiency.[10,11] Hence, it was expected that the insertion of the Sb_2S_3 layer between TiO_2 and $CH_3NH_3PbI_3$ might enhance the photovoltaic characteristics.

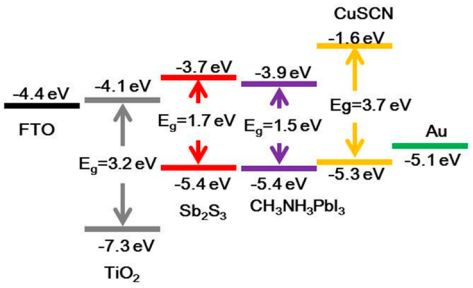

Figure 1. Energy diagram of materials for carbon-doublebond-free printed $CH_3NH_3PbI_3$ perovskite solar cells.

Special Issue: Michael Grätzel Festschrift

Received: January 15, 2014
Revised: April 29, 2014

   dx.doi.org/10.1021/jp500449z | J. Phys. Chem. C XXXX, XXX, XXX−XXX

In this report, three types of inorganic printed solar cells have been fabricated for the comparison of the photovoltaic effects, as shown in Figure 2. The first type of solar cell is ⟨TiO_2/Sb_2S_3/CuSCN/Au⟩ (Figure 2a), which was published in our recent paper.[9,12] Using a $BaTiO_3$/MgO blocking layer on TiO_2 and Ti doping in the Sb_2S_3 layer, the conversion efficiency can be improved. However, such modifications have not been applied in this report for simplification. The second type of solar cell is ⟨TiO_2/$CH_3NH_3PbI_3$/CuSCN/Au⟩ (Figure 2b). This combination with inorganic hole-transporting material (HTM) was reported as $CH_3NH_3PbI_3$ pevovskite solar cells, which can be carbon double-bond-free inorganic printed solar cells.[13] The third type of solar cell is ⟨TiO_2/Sb_2S_3/$CH_3NH_3PbI_3$/CuSCN/Au⟩ (Figure 2c), which is the new structure of this report. The insertion of the Sb_2S_3 layer at the interface of TiO_2/$CH_3NH_3PbI_3$ can improve not only the photoenergy conversion efficiency but also the stability against light exposure (AM 1.5, 100 mW cm^{-2}) without encapsulation. In order to analyze the effect of the Sb_2S_3 layer in the interface between TiO_2 and $CH_3NH_3PbI_3$ for solar cells, measurements for UV/vis absorption spectroscopy, incident photon-to-current efficiency (IPCE), X-ray diffraction (XRD), and Fourier Transform-Infrared (FT-IR) spectroscopy were performed.

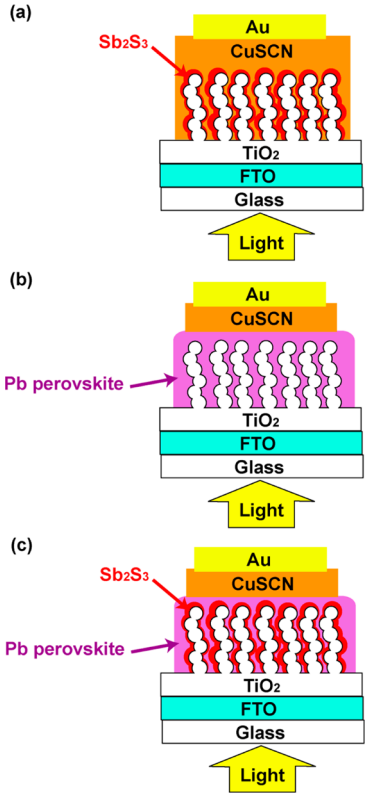

Figure 2. Structures of inorganic printed solar cells: (a) ⟨FTO/TiO_2/Sb_2S_3/CuSCN/Au⟩; (b) ⟨FTO/TiO_2/$CH_3NH_3PbI_3$/CuSCN/Au⟩; and (c) ⟨FTO/TiO_2/Sb_2S_3/$CH_3NH_3PbI_3$/CuSCN/Au⟩.

EXPERIMENTAL SECTION

TiO_2 electrodes were fabricated on F-doped SnO_2-coated glass plates [FTO; TEC-15 (t = 2 mm), NSG-Pilkington]. The edge of the FTO layer was first etched using Zn powder and HCl to eliminate shunting of the solar cell at the edge. The etched FTO substrate was put into an ultrasonic bath containing detergent, rinsed with water and ethanol, and then treated with a UV/O_3 cleaner for 15 min. Dense TiO_2 layers were coated on the FTO by spray pyrolysis using a solution of titanium diisopropoxide bis(acetylacetonate) (TAA; 0.6 mL) in ethanol (9 mL, Kanto Chemical Co., Inc., Japan) on a hot plate at 450 °C. The TAA was prepared by pouring acetylacetone (Wako Pure Chemical Industries, Ltd., Japan) into titanium isopropoxide (Kanto Chemical Co., Inc., Japan) with the ratio of 2:1 (mol/mol).

A nanocrystalline TiO_2 layer was fabricated by screen printing TiO_2 paste that was synthesized by a hydrothermal method under basic conditions and annealed at 550 °C.[14] The thickness of the nanocrystalline TiO_2 layer was ca. 2 μm. Sb_2S_3 was deposited on the nanocrystalline-TiO_2 electrodes by the chemical bath deposition (CBD) method from a solution of $SbCl_3$ and $Na_2S_2O_3$.[9,12] The as-deposited orange films of amorphous Sb_2S_3 were annealed under N_2 at 320 °C for 30 min to give a dark-brown crystalline stibnite. The samples were removed from the oven immediately after annealing and were allowed to cool in air and then were dipped into a 0.5 M aqueous KSCN solution for 5 min. The excess solution wicked off and dried at 80 °C. The Sb_2S_3 layer thickness was 1−2 nm, observed by TEM.[9] The effect of Sb_2S_3 thickness is very important to this report. The thickness of Sb_2S_3 can be controlled by varying the deposition time, which will be a further target of research.

The $CH_3NH_3PbI_3$ layer was deposited by spin coating under ambient conditions. The $CH_3NH_3PbI_3$ solution was prepared from a mixture of PbI_2 (1.1453 g, Kishida Chemical Co. Ltd., Japan) and CH_3NH_3I (0.395 g) in γ-butyrolactone (2 mL) (Kishida Chemical Co. Ltd., Japan). The CH_3NH_3I was synthesized by mixing HI (Tokyo Chemical Industry Co., Ltd., Japan) and CH_3NH_2 (Tokyo Chemical Industry Co., Ltd., Japan) according to ref 15. 40 μL of $CH_3NH_3PbI_3$ solution was dropped on the porous TiO_2 layer and spin coated at 2000 rpm for 30 s. The acceleration was 667 rpm/s. During the spin coating, hot air from a hair drier was applied to the substrate.[13] After the deposition of $CH_3NH_3PbI_3$, the substrate was annealed at 100 °C for 15 min under a N_2 flow. CuSCN (Kishida Chemical Co. Ltd., Japan) layers and Au back contacts were deposited using the doctor blade process and vacuum evaporation, respectively.[9,12]

Scanning electron microscopy (SEM; JSM-6510, JEOL) was employed to evaluate the morphology of the films. The crystal structure was characterized using X-ray diffraction (XRD; Miniflex II, Rigaku) with Cu Kα radiation. UV/vis absorption spectra were measured using a UV/vis spectrometer (Lambda 750, PerkinElmer). FT-IR spectra were measured using a FT-IR spectrometer with a diamond ATR (Frontier Optica, PerkinElmer). The size of the samples used for photocurrent−voltage (I−V) measurements was 25 mm^2 (5 × 5 mm). An AM 1.5 solar simulator equipped with a 500 W Xe lamp (YSS-80A, Yamashita Denso) was employed for photovoltaic measurements. The power of the solar simulator light was calibrated to 100 mW cm^{-2} using a reference Si photodiode (Bunkou Keiki). I−V curves were obtained by applying an external bias to the cell and measurement of the generated photocurrent with a DC voltage current source (6240, ADCMT).

RESULTS AND DISCUSSIONS

Figure 3 shows current−voltage curves of $CH_3NH_3PbI_3$-printed solar cells under light irradiation (AM 1.5, 100 mW cm^{-2}). The

dx.doi.org/10.1021/jp500449z | J. Phys. Chem. C XXXX, XXX, XXX−XXX

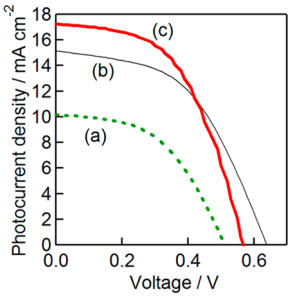

Figure 3. Photocurrent density−voltage curves of printed solar cells: (a) ⟨FTO/TiO_2/Sb_2S_3/CuSCN/Au⟩; (b) ⟨FTO/TiO_2/$CH_3NH_3PbI_3$/CuSCN/Au⟩; and (c) ⟨FTO/TiO_2/Sb_2S_3/$CH_3NH_3PbI_3$/CuSCN/Au⟩.

photovoltaic characteristics were summarized in Table 1. Although we have published 4.1% and 5.7% conversion

Table 1. Photovoltaic Effects of Printed Solar Cells Using Nanocrystalline TiO_2 Electrodes[a]

	Jsc (mA cm^{-2})	Voc (V)	FF	η (%)
(a) FTO/TiO_2/Sb_2S_3/CuSCN/Au	10.16	0.51	0.49	2.56
(b) FTO/TiO_2/$CH_3NH_3PbI_3$/CuSCN/Au	15.15	0.64	0.50	4.82
(c) FTO/TiO_2/Sb_2S_3/$CH_3NH_3PbI_3$/CuSCN/Au	17.04	0.56	0.53	5.03

[a]Each result has an average of three cells. Structures of the cells on the nanocrystalline TiO_2 electrodes are contained in Figure 3.

efficiencies using Sb_2S_3/CuSCN layers, the photovoltaic effect in Table 1a ⟨TiO_2/Sb_2S_3/ CuSCN/Au⟩ is not significant (just 2.6% conversion efficiency) because of the absence of the $BaTiO_3$/MgO blocking layer on TiO_2[9] and because of Ti doping in the Sb_2S_3 layer.[12] The solar cells of (b) ⟨TiO_2/$CH_3NH_3PbI_3$/CuSCN/Au⟩ performed high open circuit photovoltage (V_{oc}). On the other hand, (c) ⟨TiO_2/Sb_2S_3/$CH_3NH_3PbI_3$/CuSCN/Au⟩ solar cells performed high short-circuit photocurrent density (Jsc) and fill factors (FF), resulting in the highest conversion efficiency in the series of Table 1 due to the Sb_2S_3 effect. The photovoltaic characteristics of the best-efficiency cell were V_{OC}: 0.57 V, J_{SC}: 17.23 mA cm^{-2}, and *ff*: 0.52; η: 5.12%.

The light durability of inorganic printed solar cells using the $CH_3NH_3PbI_3$ layer has been examined without encapsulation (Figure 4). The examined solar cells were (a) ⟨FTO/TiO_2/$CH_3NH_3PbI_3$/CuSCN/Au⟩ and (b) ⟨FTO/TiO_2/Sb_2S_3/$CH_3NH_3PbI_3$/CuSCN/Au⟩. Without Sb_2S_3, the stability of the solar cell was very poor. The photoenergy conversion efficiency deteriorated drastically within 5 h and became very close to zero within 12 h. With Sb_2S_3, on the other hand, the conversion efficiency was maintained 65% of the initial conversion efficiency without encapsulation after the 12 h light irradiation. Therefore, the effect of the Sb_2S_3 layer in the TiO_2/$CH_3NH_3PbI_3$ interface significantly affects the photo-energy conversion efficiency (Figure 3) and the light stability (Figure 4).

Figure 5 shows the light absorption spectra of Sb_2S_3 and/or $CH_3NH_3PbI_3$ on the nanocrystalline-TiO_2 electrode in this study. The fresh layers of Sb_2S_3 and $CH_3NH_3PbI_3$ have absorption edges at 740 and 800 nm, respectively. However, after 12 h irradiation, the band edge of $CH_3NH_3PbI_3$ was

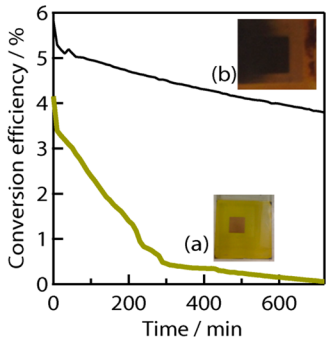

Figure 4. Variation of photoenergy conversion efficiencies of solar cells during light exposure (AM1.5, 100 mW cm^{-2}) without encapsulation in air for 12 h: (a) ⟨FTO/TiO_2/$CH_3NH_3PbI_3$/CuSCN/Au⟩ and (b) ⟨FTO/TiO_2/Sb_2S_3/$CH_3NH_3PbI_3$/CuSCN/Au⟩. The inset pictures are the photographs of cells after the light exposure.

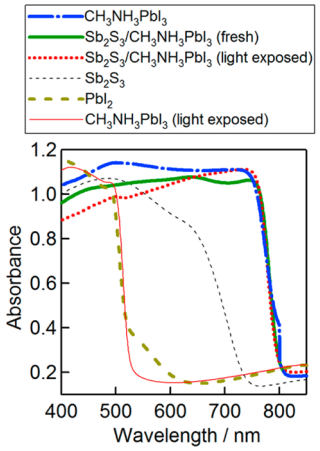

Figure 5. Reflectance absorption spectra of printed materials for solar cells on nanocrystalline-TiO_2 electrodes. The light exposure was with AM1.5 (100 mW cm^{-2}) for 12 h.

shifted to 530 nm, which was similar to PbI_2. The absorption spectrum of PbI_2 shows a shoulder from 520 to 620 nm, maybe due to the large grain on the PbI_2 layer. The spectrum of Sb_2S_3/$CH_3NH_3PbI_3$ was very close to only $CH_3NH_3PbI_3$ and did not change the absorption edge after the12 h light exposure.

Although more light has been absorbed by the cells without Sb_2S_3 than by those with Sb_2S_3 (Figure 5), the short circuit current density without Sb_2S_3 was lower than that with Sb_2S_3 (Figure 3). Therefore, it can be speculated that the internal absorbed photon-to-current conversion efficiency (APCE) with Sb_2S_3 might be higher than that without Sb_2S_3.

Figure 6 shows IPCE spectra of printed solar cells. The IPCE edge of (a) a Sb_2S_3 absorber solar cell was 740 nm. Using $CH_3NH_3PbI_3$, the IPCE edge was 800 nm. The absorption wavelength edges of Sb_2S_3 and $CH_3NH_3PbI_3$ layers (Figure 5) corresponded to the IPCE spectra edges of Sb_2S_3 and $CH_3NH_3PbI_3$ solar cells, respectively. The insertion of the Sb_2S_3 layer at the interface between TiO_2 and $CH_3NH_3PbI_3$ enhanced the IPCE value of $CH_3NH_3PbI_3$ from 50−60% to 70−80%. Moreover, the IPCE edge of the $CH_3NH_3PbI_3$ solar cell with Sb_2S_3 light exposure for 12 h was kept at 800 nm, as with the fresh solar cell. If the $CH_3NH_3PbI_3$ layer lost the photovoltaic function in the ⟨TiO_2/Sb_2S_3/$CH_3NH_3PbI_3$/CuSCN/Au⟩ cell and the resulting photovoltaic performance

dx.doi.org/10.1021/jp500449z | J. Phys. Chem. C XXXX, XXX, XXX−XXX

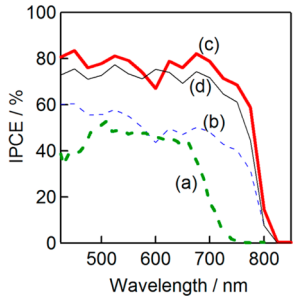

Figure 6. Incident photon-to-current efficiency (IPCE) spectra of printed solar cells: (a) ⟨FTO/TiO_2/Sb_2S_3/CuSCN/Au⟩, (b) ⟨FTO/TiO_2/$CH_3NH_3PbI_3$/CuSCN/Au⟩, (c) ⟨FTO/TiO_2/Sb_2S_3/$CH_3NH_3PbI_3$/CuSCN/Au⟩ (fresh cell), and (d) ⟨FTO/TiO_2/Sb_2S_3/$CH_3NH_3PbI_3$/CuSCN/Au⟩ [after light exposure of AM1.5 (100 mW cm^{-2}) for 12 h].

had been retained by the remaining Sb_2S_3 layer, the IPCE spectrum of (c) ⟨TiO_2/Sb_2S_3/$CH_3NH_3PbI_3$/CuSCN/Au⟩ should shift to the spectrum of (a) ⟨TiO_2/Sb_2S_3/CuSCN/Au⟩. Therefore, the Sb_2S_3 layer on the TiO_2 surface retained the photovoltaic effect of $CH_3NH_3PbI_3$.

Figure 7 shows the XRD patterns of photoactive materials (Sb_2S_3 and/or $CH_3NH_3PbI_3$) on nanocrystalline TiO_2 electrodes. XRD patterns of Sb_2S_3 and $CH_3NH_3PbI_3$ were observed in (a and b), respectively. In the (d) stacked layers of Sb_2S_3 and $CH_3NH_3PbI_3$, each crystal was observed in the XRD pattern and they were not mixed with or dispersed into each other. Although a peak of PbI_2 (at 12.6°) was observed in the (b) $CH_3NH_3PbI_3$ layer, it disappeared in the (d) Sb_2S_3/$CH_3NH_3PbI_3$ layer. It was speculated that the Sb_2S_3 layer enhanced the crystallinity of the $CH_3NH_3PbI_3$ perovskite structure and eliminated the PbI_2 hexagonal structure. In the $CH_3NH_3PbI_3$ cell exposed to light for 12 h without (c) Sb_2S_3, the crystal structure was changed from perovskite to hexagonal.[13] On the other hand, with the Sb_2S_3 addition at the interface between (e) TiO_2 and $CH_3NH_3PbI_3$, the $CH_3NH_3PbI_3$ crystal structure was retained as perovskite after the 12 h light exposure. A small peak of PbI_2 emerged again after the light exposure in the (e) Sb_2S_3/$CH_3NH_3PbI_3$ layer, which may be due to the segregation of PbI_2 by the removal of CH_3NH_2 and HI from the $CH_3NH_3PbI_3$ layer surface.

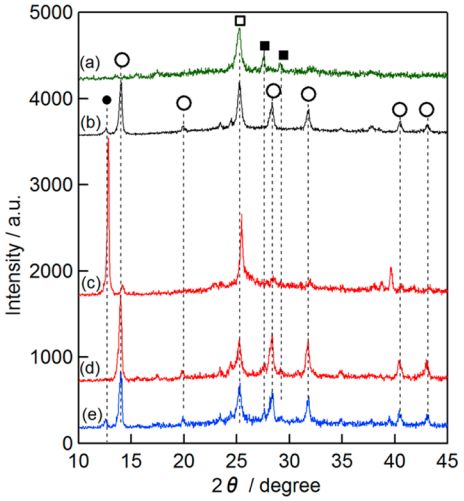

Figure 7. XRD patterns of inorganic printed photoabsorbers for solar cells on nanocrystalline-TiO_2 electrodes: (a) ⟨TiO_2/Sb_2S_3⟩, (b) ⟨TiO_2/$CH_3NH_3PbI_3$⟩ (fresh), (c) ⟨TiO_2/$CH_3NH_3PbI_3$⟩ (after light exposure for 12 h), (d) ⟨TiO_2/Sb_2S_3/$CH_3NH_3PbI_3$⟩ (fresh), and (e) ⟨TiO_2/Sb_2S_3/$CH_3NH_3PbI_3$⟩ (after light exposure for 12 h). The symbols in Figure 6 are $CH_3NH_3PbI_3$ (○), PbI_2 (●), anatase TiO_2 (□), and Sb_2S_3 (■). The light was AM1.5 (100 mW cm^{-2}).

Figure 8 shows FT-IR spectra of the $CH_3NH_3PbI_3$ layer on TiO_2: (a) in the fresh layer, (b) after 12 h of light exposure without Sb_2S_3, and (c) after 12 h of light exposure with Sb_2S_3. The apparent peaks by methylamine were observed as a line (a). Due to the thick layer of $CH_3NH_3PbI_3$, the background of TiO_2 (below 1000 nm^{-1}) was depressed, which was observed as lines (b and c). After the light exposure test without Sb_2S_3 as line (b), the layer became yellow and the FT-IR peaks of methylamine disappeared. Hence, the $CH_3NH_3PbI_3$ changed to PbI_2. On the other hand, with Sb_2S_3, the FT-IR peaks of methylamine remained as line (c). The large increase from 1000 to 3000 nm^{-1} may be attributed to H_2O adsorbed into the $CH_3NH_3PbI_3$ layer during the 12 h light exposure, which was not observed in the (a) fresh $CH_3NH_3PbI_3$ layer without H_2O adsorption or in the (b) PbI_2 layer due to the absence of $CH_3NH_3^+$. Therefore, although the top surface of CH_3NH_2 was removed from the $CH_3NH_3PbI_3$ layer, the Sb_2S_3 layer retained the $CH_3NH_3PbI_3$ perovskite crystal structure.

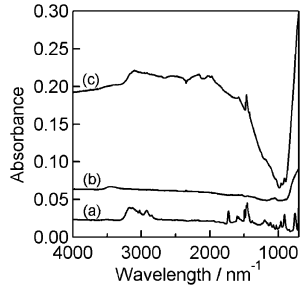

Figure 8. FT-IR spectra of (a) fresh ⟨TiO_2/$CH_3NH_3PbI_3$⟩, (b) ⟨TiO_2/$CH_3NH_3PbI_3$⟩ after light exposure for 12 h, and (c) ⟨TiO_2/Sb_2S_3/$CH_3NH_3PbI_3$⟩ after light exposure for 12 h. The light was AM1.5 (100 mW cm^{-2}).

Figure 9 shows the reaction scheme used to consider the degradation effect of the $CH_3NH_3PbI_3$ layer against the light exposure without encapsulation. Without Sb_2S_3, the $CH_3NH_3PbI_3$ layer can change to PbI_2 with losing CH_3NH_2 and HI (eq 1) by overnight light exposure (Figure 9a).

$$CH_3NH_3PbI_3 \rightleftharpoons PbI_2 + CH_3NH_2 \uparrow + HI\uparrow \quad (1)$$

On the other hand, with Sb_2S_3, the $CH_3NH_3PbI_3$ layer can be stabilized and made durable against light exposure (Figure 9b). Therefore, the decomposition of $CH_3NH_3PbI_3$ occurs at the interface between TiO_2 and $CH_3NH_3PbI_3$. TiO_2 has a strong ability to extract electrons from organic materials as photocatalysts and from iodide (I^-) as electrodes in dye-sensitized solar cells. Hence, the driving force of the decomposition may be due to the effect of electron extraction by TiO_2 from an iodide anion. The possible reaction at the TiO_2 surface may be as eqs 2–4:

$$2I^- \rightleftharpoons I_2 + 2e^- \quad [\text{at the interface between } TiO_2 \text{ and } CH_3NH_3PbI_3] \quad (2)$$

$$3CH_3NH_3^+ \rightleftharpoons 3CH_3NH_2 \uparrow + 3H^+ \quad (3)$$

dx.doi.org/10.1021/jp500449z | J. Phys. Chem. C XXXX, XXX, XXX−XXX

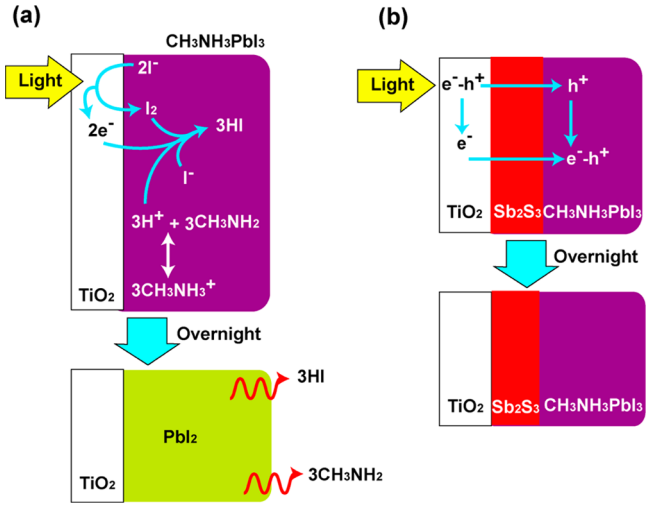

Figure 9. Degradation scheme of $CH_3NH_3PbI_3$ perovskite solar cells during light exposure test: (a) ⟨TiO_2/$CH_3NH_3PbI_3$⟩ and (b) ⟨TiO_2/Sb_2S_3/$CH_3NH_3PbI_3$⟩.

$$I^- + I_2 + 3H^+ + 2e^- \leftrightharpoons 3HI\uparrow \quad (4)$$

The $CH_3NH_3PbI_3$ perovskite crystal is composed of $CH_3NH_3^+$, Pb^{2+}, and I^- ions. At first, TiO_2 can extract electrons from I^-, resulting in I_2, which deconstructs the perovskite crystal. Equation 3 is in equilibrium. Assisted with water, the pK_a of the equation ($CH_3NH_3^+ + H_2O \leftrightharpoons CH_3NH_2 + H_3O^+$) is 10.80,[16] which suggests that the equilibrium is basically shifted to the left side but that the elimination of CH_3NH_2 and H^+ (or H_3O^+) can shift the equilibrium to the right side. Without the perovskite structure, the equilibrium (eq 3) may shift to the right side easily. The electron extracted by TiO_2 can return from the TiO_2 surface, and eq 4 can occur while emitting HI and CH_3NH_2. Losing H^+ by eq 4, the equilibrium of eq 3 can shift to the right side with the emission of CH_3NH_2 because of the low boiling point of CH_3NH_2 (17 °C).[16] In contrast, the Sb_2S_3 layer (Figure 9b) can deactivate the reaction of I^-/I_2 (eq 2) at the surface of TiO_2, the electrons can shift from the conduction band of $CH_3NH_3PbI_3$, and the $CH_3NH_3PbI_3$ layer can be stabilized and made durable against light exposure. Although the reaction of the decomposition scheme is somewhat of a speculation, it can be deduced that the presented reaction scheme is the most probable one due to the results shown above. In order to provide concrete evidence, we are managing further research at present.

The improvement in PCE should be attributed directly to improvement in V_{OC} by the buffering sulfides.[11] However, this same improvement is not observed in the devices reported in this article; specifically, the device without Sb_2S_3 has a greater V_{oc} (0.64 V) than the device with Sb_2S_3 (0.56 V). Instead, here, the improvement in overall device performance seems to be a result of increased short circuit current density and fill factor rather than V_{OC}. Therefore, it was thought that the improvement of the photovoltaic effect and the stability of the Sb_2S_3 layer were due not only to the buffering effect but also to the passivation effect of the TiO_2 photocatalysis. Without Sb_2S_3, the holes generated in the TiO_2 conduction band by UV irradiation can extract electrons from an I^- anion in the Pb perovskite layer, resulting in Pb perovskite crystal decomposition. With the Sb_2S_3 layer, on the other hand, the charge extraction from the I^- anion to the TiO_2 conduction band can be prohibited, resulting in the enhancement of the charge recombination and a decrease in the V_{OC}. However, this prohibition of the TiO_2 photocatalysis may enhance the stability of the perovskite layer.

In conclusion, $CH_3NH_3PbI_3$ perovskite solar cells using an inorganic hole transporting material (CuSCN) with/without Sb_2S_3 by chemical bath deposition at the interface between TiO_2 and $CH_3NH_3PbI_3$ were fabricated. The Sb_2S_3 layer was improved for higher photovoltaic effects. Light exposure tests of $CH_3NH_3PbI_3$ perovskite solar cells have been performed without encapsulation. During the light exposure test without Sb_2S_3, the black $CH_3NH_3PbI_3$ layers were completely changed to yellow, because the perovskite $CH_3NH_3PbI_3$ was changed to hexagonal PbI_2. With Sb_2S_3, on the other hand, the $CH_3NH_3PbI_3$ perovskite solar cells did not change structures (measured by XRD), and the wavelength edges of absorption and IPCE spectra also did not change. Therefore, it was understood that Sb_2S_3 elongates the lifetime of the $CH_3NH_3PbI_3$ perovskite structure during light exposure and that the degradation origin of the $CH_3NH_3PbI_3$ perovskite layer is the interface between TiO_2 and $CH_3NH_3PbI_3$. The degradation is related to the unfixed positioning of the $CH_3NH_3^+$ cation in the $CH_3NH_3PbI_3$ perovskite crystal.[17−19] However, the degradation effect by water is still not clear. Bromide doping enhanced the stability of the $CH_3NH_3PbX_3$ solar cells against moisture.[3] At the same time, water should affect the lithium salt doped in the HTM layer for the $CH_3NH_3PbX_3$ solar cells. The photovoltaic performance after 12 h has not been checked. After using a very stable device, the light stability after over 1000 h shall be checked in the further research. Further investigation is necessary to understand the inside of the degradation mechanism.

AUTHOR INFORMATION

Corresponding Author

*E-mail: itou@eng.u-hyogo.ac.jp. Tel/Fax: +81-79-267-4858.

Notes

The authors declare no competing financial interest.

ACKNOWLEDGMENTS

Part of this research was supported by the Advanced Low Carbon Technology Research and Development Program (ALCA, JST, Japan).

REFERENCES

(1) Kim, H. S.; Lee, C. R.; Im, J. H.; Lee, K. B.; Moehl, T.; Marchioro, A.; Moon, S. J.; Humphry-Baker, R.; Yum, J. H.; Moser, J. E.; et al. Lead Iodide Perovskite Sensitized All-Solid-State Submicron Thin Film Mesoscopic Solar Cell with Efficiency Exceeding 9%. *Sci. Rep.* **2012**, *2*, 591.

(2) Lee, M. M.; Teuscher, J.; Miyasaka, T.; Murakami, T. N.; Snaith, H. J. Efficient Hybrid Solar Cells Based on Meso-Superstructured Organometal Halide Perovskites. *Science* **2012**, *338*, 643−647.

(3) Noh, J. H.; Im, S. H.; Heo, J. H.; Mandal, T. N.; Seok, S. I. Chemical Management for Colorful, Efficient, and Stable Inorganic−Organic Hybrid Nanostructured Solar Cells. *Nano Lett.* **2013**, *13*, 1764−1769.

(4) Burschka, J.; Pellet, N.; Moon, S. J.; Humphry-Baker, R.; Gao, P.; Nazeeruddin, M. K.; Grätzel, M. Sequential Deposition as a Route to High-Performance Perovskite-Sensitized Solar Cells. *Nature* **2013**, *499*, 316−319.

(5) Liu, D.; Kelly, T. L. Perovskite Solar Cells with a Planar Heterojunction Structure Prepared Using Room-Temperature Solution Processing Techniques. *Nat. Photonics* **2014**, *8*, 133−138.

(6) Wang, J. T.-W.; Ball, J. M.; Barea, E. M.; Abate, A.; Alexander-Webber, J. A.; Huang, J.; Saliba, M.; Mora-Sero, I.; Bisquert, J.; Snaith,

H. J.; et al. Low-Temperature Processed Electron Collection Layers of Graphene/TiO_2 Nanocomposites in Thin Film Perovskite Solar Cells. *Nano Lett.* **2014**, *14*, 724−730.
(7) Perera, S.; Senadeera, R.; Tennakone, K.; Ito, S.; Kitamura, T.; Wada, Y.; Yanagida, S. The Effect of MgO on the Enhancement of the Efficiency in Solid-State Dye Sensitized Photocells Fabricated with SnO_2 and CuI. *Bull. Chem. Soc. Jpn.* **2003**, *76*, 659−662.
(8) Ito, S.; Makari, Y.; Kitamura, T.; Wada, Y.; Yanagida, S. Fabrication and Characterization of Mesoporous SnO_2/ZnOcomposite Electrodes for Efficient Dye Solar Cells. *J. Mater. Chem.* **2004**, *14*, 385−390.
(9) Tsujimoto, K.; Nguyen, D.-C.; Ito, S.; Nishino, H.; Matsuyoshi, H.; Konno, A.; Kumara, G. R. A.; Tennakone, K. TiO_2 Surface Treatment Effects by Mg^{2+}, Ba^{2+}, and Al^{3+} on Sb_2S_3 Extremely Thin Absorber Solar Cells. *J. Phys. Chem. C* **2012**, *116*, 13465−13471.
(10) Eisgruber, I. L.; Granata, J. E.; Sites, J. R.; Hou, J.; Kessler, J. Blue-Photon Modification of Nonstandard Diode Barrier in $CuInSe_2$ Solar Cells. *Sol. Energy Mater. Sol. Cells* **1998**, *53*, 367−377.
(11) Gloeckler, M.; Sites, J. R. Efficiency Limitations for Wide-Band-Gap Chalcopyrite Solar Cells. *Thin Solid Films* **2005**, *480*−*481*, 241−245.
(12) Ito, S.; Tsujimoto, K.; Nguyen, D.-C.; Manabe, K.; Nishino, H. Doping Effects in Sb_2S_3 Absorber for Full-Inorganic Printed Solar Cells with 5.7% Conversion Efficiency. *Int. J. Hydrogen Energy* **2013**, *38*, 16749−16754.
(13) Ito, S.; Tanaka, S.; Vahlman, H.; Nishino, H.; Manabe, K.; Lund, P. Structural Control and Aging Effects of Nanocrystalline TiO_2/$CH_3NH_3PbI_3$ with CuSCN Hole Conductor as Inorganic Printed Solar Cell. *ChemPhysChem* **2014**, *15*, 1194−1200.
(14) Ito, S.; Zakeeruddin, S. M.; Comte, P.; Liska, P.; Kuang, D.; Grätzel, M. *Nat. Photonics* **2008**, *2*, 693−696.
(15) Etgar, L.; Gao, P.; Xue, Z.; Peng, Q.; Chandiran, A. K.; Liu, B.; Nazeeruddin, M. K.; Grätzel, M. *J. Am. Chem. Soc.* **2012**, *134*, 17396−17399.
(16) Ouellette, R. J. *Organic Chemistry: A Brief Introduction*, 2nd ed.; Prentice Hall: Upper Saddle River, NJ.
(17) Mosconi, E.; Amat, A.; Nazeeruddin, M. K.; Grätzel, M.; De Angelis, F. First-Principles Modeling of Mixed Halide Organometal Perovskites for Photovoltaic Applications. *J. Phys. Chem. C* **2013**, *117*, 13902−13913.
(18) Wasylishen, R. E.; Knop, O.; Macdonald, J. B. Cation Rotation in Methyl Ammonium Lead Halides. *Solid State Commun.* **1985**, *56*, 581−582.
(19) Poglitsch, A.; Weber, D. Dynamic Disorder in Methylammoniumtrihalogenoplumbates (II) Observed by Millimeterwave Spectroscopy. *J. Chem. Phys.* **1987**, *87*, 6373−6378.